Article:
De Motte, RA, Barker, R orcid.org/0000-0002-5106-6929, Burkle, D et al. (2 more authors) (2018) The early stages of $FeCO_3$ scale formation kinetics in corrosion. Materials Chemistry and Physics, 216. pp. 102-111. ISSN 0254-0584

https://doi.org/10.1016/j.matchemphys.2018.04.077

Accepted Manuscript

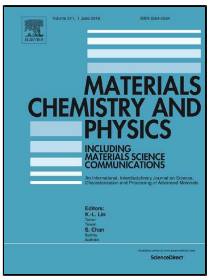

The early stages of $FeCO_3$ scale formation kinetics in CO_2 corrosion

R.A. De Motte, R. Barker, D. Burkle, S.M. Vargas, A. Neville

PII:	S0254-0584(18)30346-8
DOI:	10.1016/j.matchemphys.2018.04.077
Reference:	MAC 20572
To appear in:	*Materials Chemistry and Physics*
Received Date:	24 August 2017
Revised Date:	18 April 2018
Accepted Date:	22 April 2018

Please cite this article as: R.A. De Motte, R. Barker, D. Burkle, S.M. Vargas, A. Neville, The early stages of $FeCO_3$ scale formation kinetics in CO_2 corrosion, *Materials Chemistry and Physics* (2018), doi: 10.1016/j.matchemphys.2018.04.077

The Early Stages of $FeCO_3$ Scale Formation Kinetics in CO_2 Corrosion

R.A. De Motte, [1a)] R. Barker,[1] D. Burkle, [1] S.M. Vargas, [2] and A. Neville, [1]

[1]*Insititute of Functional Surfaces (iFS), School of Mechanical Engineering, University of Leeds, Leeds LS2 9JT, United Kingdom*
[2]*BP America, Inc., Houston Texas 77079*

Keywords: CO_2 Corrosion; $FeCO_3$ nucleation and growth; Precipitation kinetics; X65 carbon steel.

Abstract: In a carbon dioxide (CO_2) corrosive environment, when the product of the local concentrations of iron (Fe^{2+}) and carbonate (CO_3^{2-}) ions exceed the solubility limit, the precipitation of iron carbonate ($FeCO_3$) on the internal walls of carbon steel pipelines can significantly reduce the corrosion rate. In the following work, static glass cell corrosion experiments were conducted to understand the precipitation behavior in the early stages of $FeCO_3$ development and the factors favorable to protective film formation. The corrosion and precipitation rates were followed using a combination of mass gain, mass loss, electrochemistry and surface analysis techniques. At the conditions studied, the protectiveness and the rate of film formation was observed to vary significantly. The results indicated that the early stages of $FeCO_3$ precipitation consists of a complex simultaneous nucleation and growth process. $FeCO_3$ precipitation is shown to be dependent on surface species concentrations which can be significantly different to that of the bulk solution. Additionally, the role of crystal surface coverage and the blocking of actively corroding sites on the steel surface is examined and is shown to play a critical role in reducing precipitation kinetics at low levels of bulk super-saturation.

1. Introduction

CORROSION is a key hindrance to the successful transportation of hydrocarbons in the oil and gas industry. Its occurrence degrades pipelines which in turn can result in major financial and environmental implications. One of the most frequent and significant internal corrosion problems experienced in oil and gas pipelines is carbon dioxide (CO_2) corrosion, which is also referred to as 'sweet' corrosion [1]. The corrosion mechanism consists of a series of simultaneous chemical, electrochemical and transport processes. Table 1 shows a list of the main chemical equilibrium reactions and their associated equilibrium constants that are generally agreed to occur in an aqueous CO_2 corrosive environment [2].

Reaction	Equilibrium Constant	
$CO_{2(g)} \leftrightarrow CO_{2(aq)}$	$K_{sol} = [CO_2]/p_{CO2}$	(1)
$K_{sol} = \frac{14.5}{1.00258} \times 10^{[-(2.27 + 5.65 \times 10^{-3} T_f - 8.06 \times 10^{-6} T_f^2 + 0.075I)]}$ molar/bar [3]		(2)
$CO_{2(aq)} + H_2O_{(aq)} \leftrightarrow H_2CO_{3(aq)}$	$K_{hy} = [H_2CO_3]/[CO_2]$	(3)
$K_{hy} = 2.58 \times 10^{-3}$ [4]		(4)
$H_2CO_{3(aq)} \leftrightarrow H^+_{(aq)} + HCO_3^-{}_{(aq)}$	$K_{ca} = [H^+][HCO_3^-]/[H_2CO_3]$	(5)
$K_{ca} = 387.6 \times 10^{[-(6.41 - 1.59 \times 10^{-3} T_f + 8.52 \times 10^{-6} T_f^2 - 3.07 \times 10^{-5} p - 0.4772 I^{1/2} + 0.1180I)]}$ molar [3]		(6)
$HCO_3^-{}_{(aq)} \leftrightarrow H^+_{(aq)} + CO_3^{2-}{}_{(aq)}$	$K_{bi} = [H^+][CO_3^{2-}]/[HCO_3^-]$	(7)
$K_{bi} = 10^{[-(10.61 - 4.97 \times 10^{-3} T_f + 1.331 \times 10^{-5} T_f^2 - 2.624 \times 10^{-5} p - 1.166 I^{1/2} + 0.3466I)]}$ molar [3]		(8)

Table 1. Chemical equilibrium reactions and their equilibrium constants in CO_2-H_2O systems where T_f is temperature in degrees Fahrenheit, I is the molar ionic strength and p is the total pressure in psi[2].

Corrosion is an electrochemical process and involves the transfer of electrons at the metal-solution interface. There are four possible cathodic reactions that may take place in CO_2-containing solutions that have been discussed in literature [5-7] and are shown in Equations (9-12). The dissociation of H_2CO_3, expressed in Equations (5) and (7), serves as a source of H^+ ions which are subsequently reduced at the surface according to Equation (9). In addition, there is also the possibility of the direct reduction of H_2CO_3 (Equation (10)), the direct reduction of bicarbonate ion (Equation (11)) and the direct reduction of water (Equation (12)). The exact cathodic reaction that takes place at the steel surface has been the subject of some debate. It is generally agreed that carbonic acid, H_2CO_3 would dissociate into hydrogen faster than the respective species could diffuse to the surface of the steel in a pH range 3 to 5.5. However, at a more alkaline pH, the other contributions mentioned may be considered to be significant due to the limited flux of H^+ ions [8,9].

H_2 evolution	$2H^+_{(aq)} + 2e^- \rightarrow H_{2(g)}$	(9)
Direct reduction of H_2CO_3 (or 'buffering effect')	$2H_2CO_{3(aq)} + 2e^- \rightarrow H_{2(g)} + 2HCO_3^-{}_{(aq)}$	(10)
Bicarbonate reduction	$2HCO_3^-{}_{(aq)} + 2e^- \rightarrow H_{2(g)} + 2CO_3^{2-}{}_{(aq)}$	(11)
Water reduction	$2H_2O_{(l)} + 2e^- \rightarrow H_{2(g)} + 2OH^-_{(aq)}$	(12)

The electrochemical dissolution of iron is the dominant anodic reaction in CO_2 corrosion. The reaction comprises of multi-step reactions [10] with various intermediate products. However, Equation (13) is considered the overall anodic reaction.

$$Fe_{(s)} \rightarrow Fe^{2+}_{(aq)} + 2e^{-} \tag{13}$$

From the description of the electrochemical processes, it is clear that a direct result of the CO_2 corrosion process is the increase in the presence of Fe^{2+} ions in the process fluid. At a certain instant in time, depending on the environmental conditions, the product of concentrations of Fe^{2+} and CO_3^{2-} ions exceed the iron carbonate solubility limit (K_{sp}) and the precipitation of solid iron carbonate ($FeCO_3$) becomes thermodynamically favorable (Equation (14)) [11,12]. Under these conditions, $FeCO_3$ is reported to precipitate onto the corroding surface and protect the underlying surface from further corrosion.

$$Fe^{2+}_{(aq)} + CO^{2-}_{3\,(aq)} \rightarrow FeCO_{3(s)} \tag{14}$$

A parameter used frequently in literature [11,12] to identify the nature, morphology and protection of the $FeCO_3$ precipitation process is the saturation ratio (SR) which is the ratio of the product of the relevant species to the solubility product of iron carbonate and is defined by Equation (15).

$$SR = \frac{\left[Fe^{2+}\right]\left[CO_3^{2-}\right]}{K_{sp}} \tag{15}$$

where $[Fe^{2+}]$ is the concentration of iron ions (in mol/L) and $[CO_3^{2-}]$ is the concentration of carbonate ions (in mol/L). K_{sp} is the solubility product of $FeCO_3$ (in mol^2/L^2) and has been defined by different models [14-16] as a function of temperature. However, in a more recent study by Sun et al. [12,13], a correlation that defines the $FeCO_3$ solubility product as a function of both temperature and ionic strength (I) was proposed and is shown in Equation (16). The correlation was stated to have agreed more effectively with experimental data and has been used in many of the more recent studies in $FeCO_3$ precipitation [13-15].

$$\log K_{sp} = -59.3498 - 0.041377T_k - \frac{2.1963}{T_k} + 24.5724\log_{10}(T_k) + 2.518I^{0.5} - 0.657I \tag{16}$$

In recent literature [12-16], there has been a significant interest in furthering the quantitative understanding of $FeCO_3$ precipitation kinetics. Accurately predicting the rate of scale growth requires an extensive understanding of the nucleation and growth processes in relation to the local solution chemistry and can provide significant strides in corrosion management if correctly determined. Semi-empirical growth rate expressions have been developed in the past to predict the $FeCO_3$ precipitation rate (PR) in a CO_2 corrosive environment [12-16]. These equations all take the following form:

$$PR = k_r \frac{A}{V} \sigma^r \tag{17}$$

where k_r is an experimentally determined kinetic constant (in the form of a temperature dependent Arrhenius function), A/V is surface area-to-volume ratio, σ is the driving force and r is the reaction order. The models, proposed in literature, vary from one another based on differences in their experimental

methods and are shown to predict precipitation rates which differ by 1-3 orders of magnitude over a range of temperature and saturation ratio values [12]. Furthermore, the driving force for crystallization within these models is described in terms of the SR of the bulk solution (i.e. not at the surface of the sample), yet some authors [17] have suggested and demonstrated that the surface concentration of species is vitally important in determining precipitation kinetics and can be vastly different to that of the bulk solution for a corroding steel surface.

This work seeks to examine the early stages of nucleation and growth of $FeCO_3$ films through a series of 20 hour static experiments to identify the level of protectiveness offered and the characteristics of their development. The study focuses on the analysis of the behavior of freely corroding samples without the introduction of iron chloride into the bulk solution to promote crystal growth. The effect of pH on CO_2 corrosion at temperatures up to 100°C has been described by Nesic et al. [18,19] and has been shown to have a significant effect on both the corrosion rate and $FeCO_3$ film formation. Consequently, solution pH was chosen to be varied within this study and the two conditions of pH evaluated were carefully chosen to compare and contrast the nucleation and growth characteristics of $FeCO_3$ crystals. The purpose of this work is to systematically follow the growth of $FeCO_3$ in the early stages whilst also recording the bulk SR in an effort to further understand $FeCO_3$ precipitation and identify the underlying factors which influence the kinetics and development of protective films.

2. Experimental Procedure

All experiments were conducted in a glass cell as shown in Figure 1 and were performed in static conditions at atmospheric pressure. The glass cell was filled with 1 litre of distilled water containing 3.5 wt% sodium chloride (NaCl) and heated to the desired temperature of 80°C. The temperature was maintained at ±1°C through the use of a temperature probe connected to a hotplate forming a feedback loop. To achieve de-aeration and minimize the dissolved oxygen concentration, the test solution was purged with CO_2 gas for a minimum of 4 hours prior to each experiment. In addition, CO_2 was continuously bubbled into the test solution throughout the entire duration of each experiment. After the solution was deoxygenated, the pH was increased to the desired value of pH 6.3 or pH 6.8 through the addition of sodium bicarbonate ($NaHCO_3$). In order to achieve a consistent value of pH, a mass of 4g and 8g of $NaHCO_3$ was added to the test solution to attain a pH of 6.3 and 6.8 respectively. A magnetic stirrer, rotating at a speed of 200 rpm, was used continuously throughout the experiment to promote chemical consistency within the fluid.

The working specimens were cylindrical samples of X65 carbon steel, 25 mm in diameter with an exposed surface area of 4.9 cm^2. The chemical composition of the X65 carbon steel samples used is shown in Table 2. Prior to immersion, the specimen surfaces were wet-ground successively with 120, 320 and 600 grit silicon carbide paper, degreased with acetone and rinsed with distilled water before being dried using compressed air.

C	Mn	Si	P	S	Cr	Cu	Ni	Mo	Al
0.05	1.32	0.31	0.013	0.002	0.042	0.019	0.039	0.031	0.032

Table 2. X65 carbon steel chemical composition.

Experiments were carried out with one sample per test cell using either electrochemical techniques to monitor *in situ* corrosion rate or the mass gain/loss method to validate corrosion measurements and determine the mass of $FeCO_3$ precipitated.

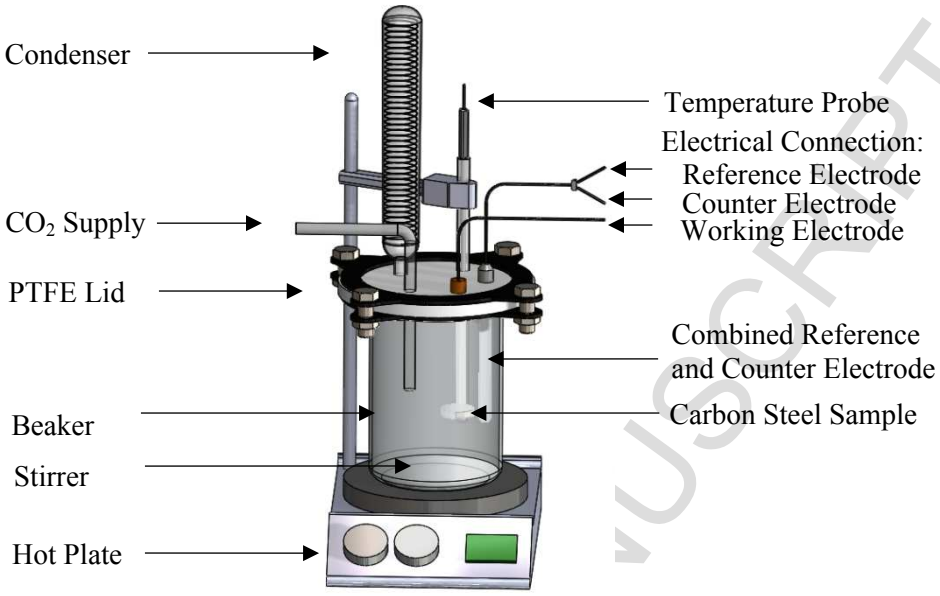

Figure 1. Labelled schematic of static experimental set-up.

2.1. Electrochemical measurements

Electrochemical experiments were conducted using a conventional three-electrode setup with a carbon steel sample serving as the working electrode and a combined redox electrode consisting of a Ag/AgCl reference electrode and a platinum counter electrode. The electrodes were connected to a potentiostat (ACM Gill) and the corrosion process was monitored by means of the linear polarization resistance (LPR) technique. The polarization resistance (R_p) was obtained by polarizing the working electrode ±15 mV from open-circuit potential (OCP) and scanning at a rate of 0.25 mV/s. LPR measurements were undertaken every 15 minutes over a total time of 20 hours. A Stern-Geary coefficient value of 15.2 was used in all cases to calculate the LPR corrosion rate and was determined based on a theoretical model by Stern et al.[20,21]. The R_p was corrected for Ohmic drop using the solution resistance measured by Electrochemical Impedance Spectroscopy.

2.2. Mass gain/loss measurement

Mass gain/loss experiments were conducted over varying time periods of 2, 5, 10, 15 and 20 h. Each test was conducted separately with one sample present over the different time periods. Both the precipitation rate (accumulation rate of the corrosion product layer) and the corrosion rate of the mild steel sample was measured by the mass change method [12,13]. Measurements were taken of the mass of the sample prior to running the experiment (m_1), at the end of the experiment with $FeCO_3$ scale present on the surface (m_2) and after the corrosion product was removed using Clarke's solution (m_3). The mass loss from corrosion was obtained by subtracting m_3 from m_1 and mass gain from precipitation was obtained by subtracting m_3

from m_2. The time averaged precipitation rate was calculated according to Equation (18), with a similar approach being applied to determine the corrosion rate.

$$PR = \frac{m_2 - m_3}{MW_{FeCO3} \times t \times A \times 3600} \quad (18)$$

where PR is the precipitation rate (mol/m^2·s), mass m_2 and m_3 is the mass of the sample before and after the $FeCO_3$ scale is chemically removed (g), MW_{FeCO3} is the molecular weight of $FeCO_3$ (g/mol), t is the exposed time (h) and A is the exposed sample area (m^2).

At the end of each experiment, the samples were rinsed with acetone, dried and retained in a desiccator prior to post surface analysis in the form of Scanning Electron Microscopy (SEM) and X-Ray Diffraction (XRD). Samples of the solution were also extracted at different time intervals to measure the ferrous ion concentration in the bulk solution using ultraviolet-visible (UV-vis) spectrophotometry.

3. Results

The effect of pH on the corrosion rate and $FeCO_3$ formation was determined for a static CO_2 environment at 80°C, atmospheric pressure and 3.5 wt% NaCl with no addition of Fe^{2+} ions to the bulk solution. The LPR corrosion rate results as a function of time for experiments conducted at solution pH 6.3 and pH 6.8 are shown in Figure 2. All experiments were repeated at least three times to indicate the reproducibility of the results. Each data point within the figure provides the averages across all repeats with the error bars denoting the maximum and the minimum values recorded.

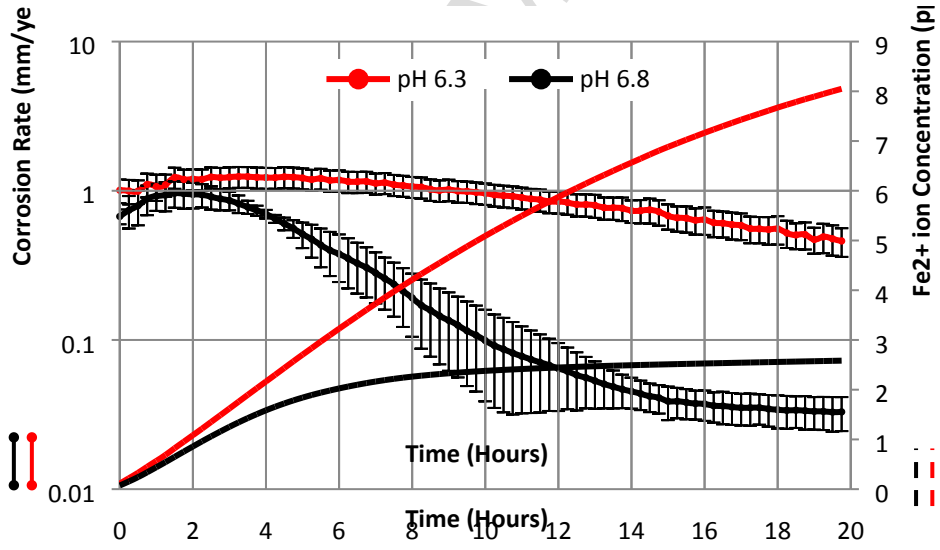

Figure 2. Effect of pH on CO_2 corrosion of X65 carbon steel and resulting cumulative bulk Fe^{2+} ion concentration based on the assumption that all ferrous ions produced are released into the bulk and no precipitation occurs in the system.

Figure 2 shows that at pH 6.3, a minor decrease in the corrosion rate was observed over the 20 hour period. However, at pH 6.8, a more significant and faster decline in the corrosion rate was observed. The final corrosion rates at the end of 20 hours was recorded to be on average 0.03 mm/year and 0.46 mm/

year for pH 6.8 and pH 6.3 respectively. The more significant reduction in the corrosion rate at pH 6.8 is an indication of a more protective film being formed more rapidly in the given time frame. The secondary axis within Figure 2 depicts the Fe^{2+} concentration in the bulk solution as a result of the corrosion process. The trend is represented by a dashed line to differentiate from the primary axis data. The values are arithmetically determined and show the total Fe^{2+} ions introduced into the system as a result of the corrosion of the mild steel surface. The results indicate that the more protective film is associated with the system with a lower cumulative flux of Fe^{2+} into the system over time. However, it is important to be noted, the Fe^{2+} concentrations calculated in Figure 2 are an overestimation of the concentration in the bulk solution as, in a real system, scale precipitation is expected to occur at the steel surface and potentially also within the bulk solution.

Figures 3 (a) and (b) show the results of the XRD analysis carried out in order to confirm the identity of the phases which constitute the film formed at pH 6.3 and pH 6.8, respectively. The XRD patterns illustrate that mainly Fe (from the steel substrate) and $FeCO_3$ were detected on the surface for both conditions of pH. This analysis confirms that the corrosion product layer formed on the mild steel surface within this study is $FeCO_3$.

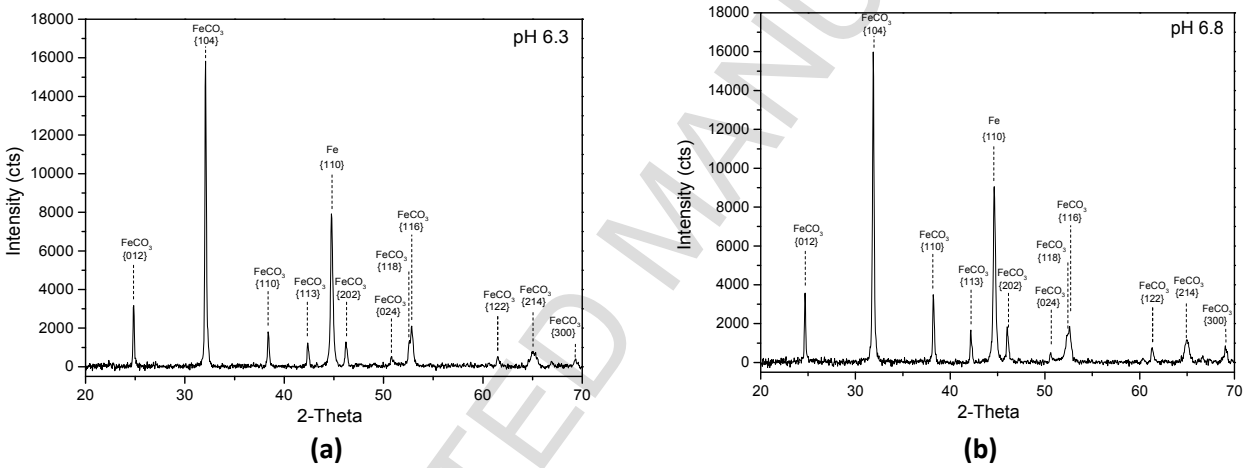

Figure 3. XRD patterns of X65 carbon steel exposed to a CO_2-saturated 3.5 wt.% NaCl brine at 80°C and (a) pH 6.3 and (b) pH 6.8 for 20 hours.

In addition to the 20 hour electrochemical measurements, mass change experiments were also conducted for time periods of 2, 5, 10, 15 and 20 hours under identical conditions to track the development of the $FeCO_3$ crystals and their surface coverage over time. From the results of the XRD analysis, the mass gain measurements made under these conditions can be assumed to accurately reflect the mass of $FeCO_3$ on the steel surface. Figure 4 shows the mass gain (relating to precipitation) and mass loss (relating to corrosion) measurements at the end of each time period for a pH of 6.3 and 6.8. This is supported by SEM images in Figures 5 and 6.

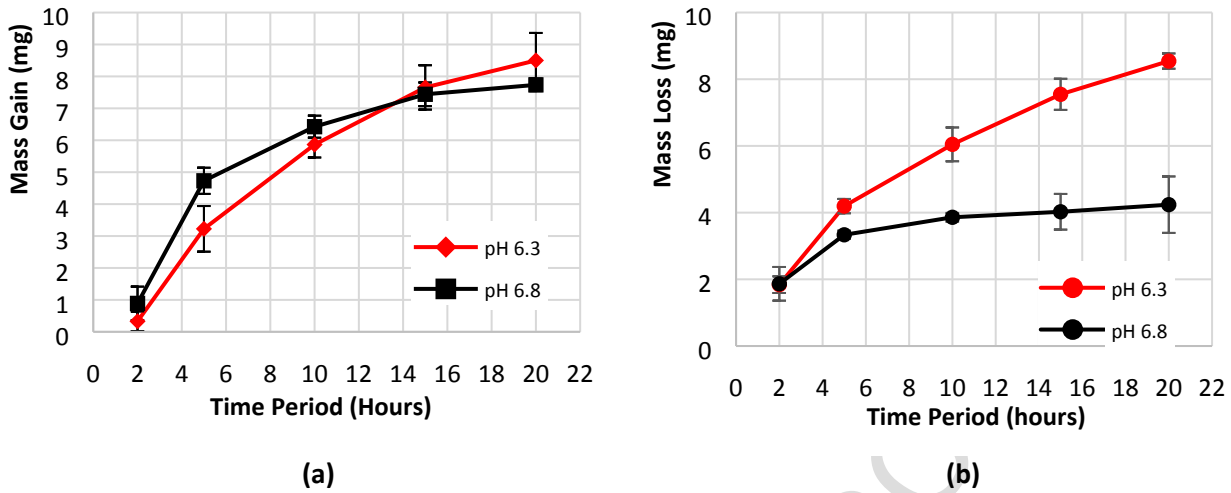

Figure 4. (a) Mass gain due to $FeCO_3$ precipitation. (b) Mass loss due to corrosion at pH 6.3 and pH 6.8 over variable time periods of 2, 5, 10, 15 and 20 hours.

Figure 4(a) shows that the mass gain is higher for a pH of 6.8 at the earlier time periods. However, over longer time periods, the rate of precipitation decreases. The mass gain at pH 6.3 continues to increase and exceeds the values measured at pH 6.8 at the end of the 20 hour period. From the LPR measurements in Figure 2, it was observed that a significantly more protective $FeCO_3$ film forms at pH 6.8 compared to pH 6.3 after 20 hours. Therefore, the mass change results show that the protectiveness of the $FeCO_3$ film cannot be directly related to the quantity of $FeCO_3$ on the steel surface. This indicates that a higher level of understanding is required in relation to the precipitation behavior as opposed to merely its formation kinetics to accurately predict film protectiveness. Figure 4(b) shows that the mass loss is progressively greater for pH 6.3 in comparison to pH 6.8, corroborating with the *in situ* LPR measurements shown in Figure 2.

Figures 5 and 6 show selected SEM images taken at the end of the specific time periods of 2, 5, 10, 15 and 20 hours. Multiple images were taken across the samples to attain an overall representation of surface coverage. The figures show representative images of approximately 175×175 μm^2 area of the sample surfaces. At both conditions of pH, crystals are observed to nucleate and grow on the sample surface but with a clear differences in their formation. The development of the layer is observed to be not confined to discrete periods of nucleation and growth as both processes are observed to be occurring simultaneously resulting in a varying distribution of crystal sizes across the steel surface, particularly at pH 6.8. The figures show that the crystals are more discrete and larger in size at pH 6.3 at all time periods with crystals as large as 40 µm being formed after 20 hours. However, at pH 6.8, the maximum crystal size was observed to be approximately half this size indicating a contrasting growth behavior. The images were taken at the same magnification and the difference in density and compactness of the film formed at each pH is clear. Figure 5 shows that at pH 6.3, fewer $FeCO_3$ crystals are observed across the mild steel surface in comparison to Figure 6 which shows a more compact and dense crystal formation after 20 hours. The greater extent of crystal coverage at pH 6.8 compared to pH 6.3 correlates with the lower corrosion rate measured (Figure 2).

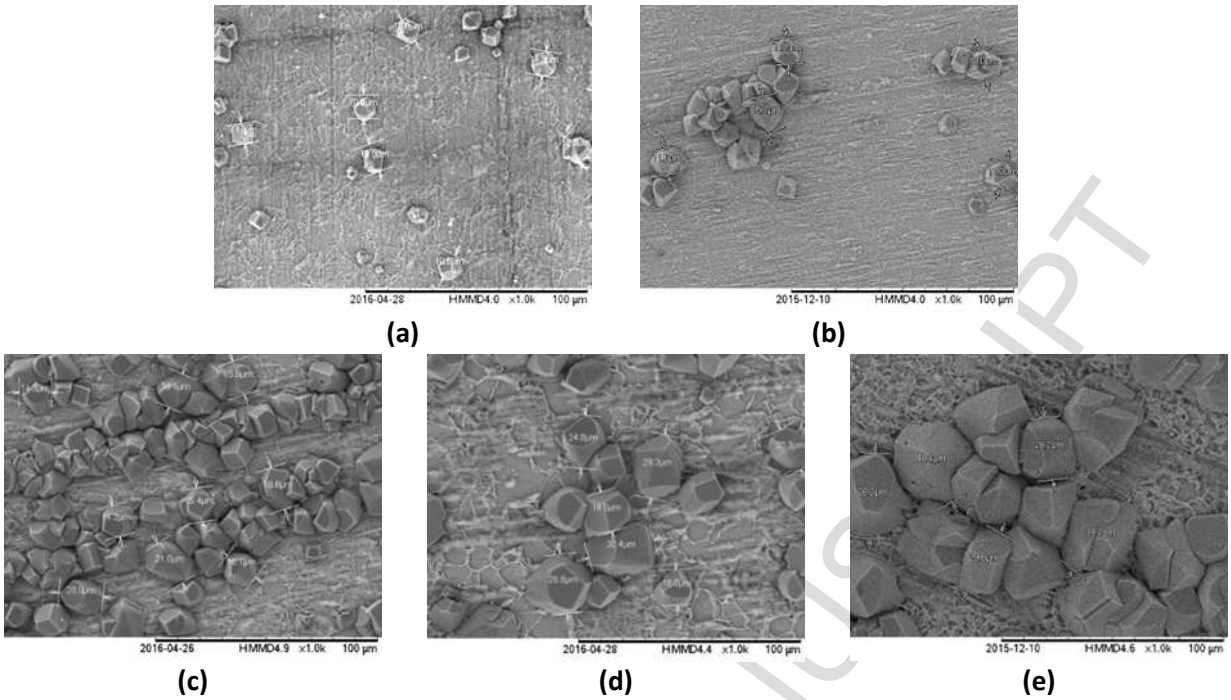

Figure 5. SEM images illustrating $FeCO_3$ crystal formation over time on X65 carbon steel at pH 6.3. Images are after (a) 2 h, (b) 5 h, (c) 10 h, (d) 15 h and (e) 20 h.

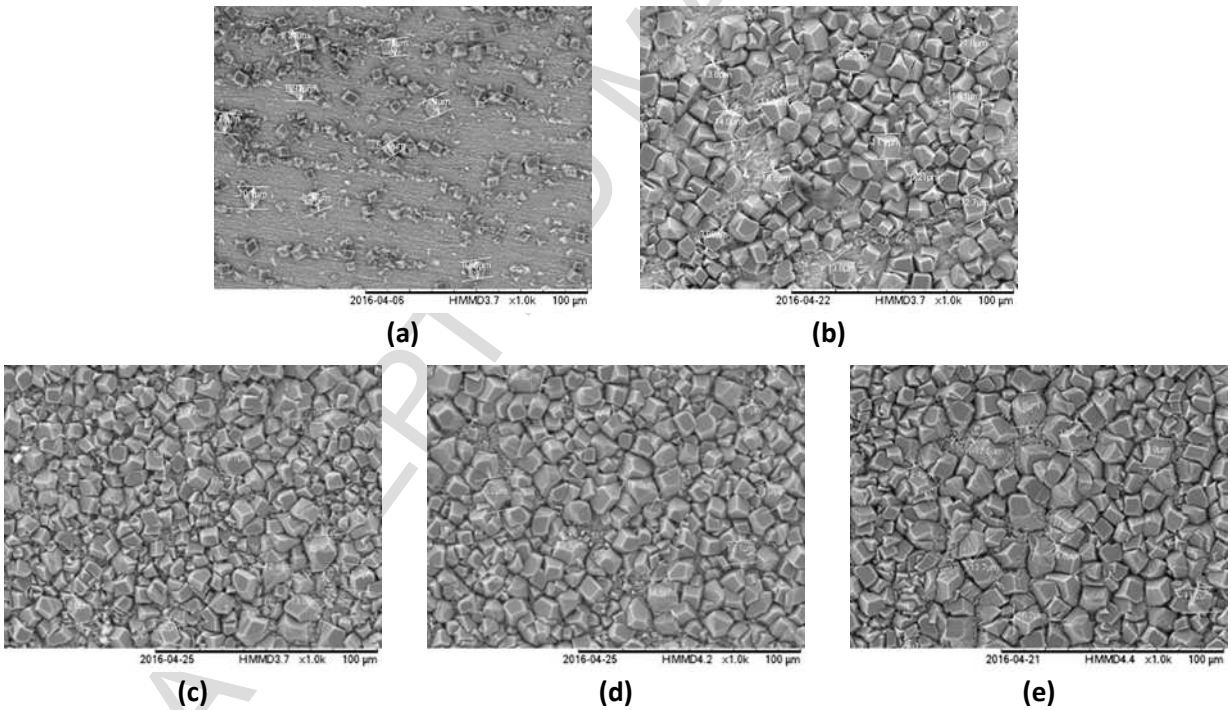

Figure 6. SEM images illustrating $FeCO_3$ crystal formation over time on X65 carbon steel at pH 6.8. Images are after (a) 2 h, (b) 5 h, (c) 10 h, (d) 15 h and (e) 20 h.

The multiple SEM images taken across the surface were carefully analyzed to determine the varying crystal size and surface coverage. Figure 7(a) compares the average crystal size as a function of time for pH 6.3 and pH 6.8 while Figure 7(b) compares the percentage surface coverage with the percentage

reduction in corrosion rate over time for both conditions of pH studied. The crystal size was determined using SEM image analysis software to measure the size of each individual crystal. An average of the varying crystal sizes was determined across the images taken at the end of each time period for a pH of 6.3 and 6.8. Results show that the crystal size increases much more rapidly at pH 6.3 whereas the growth of crystals are more limited at pH 6.8 where only a slight increase in average crystal size is observed over time.

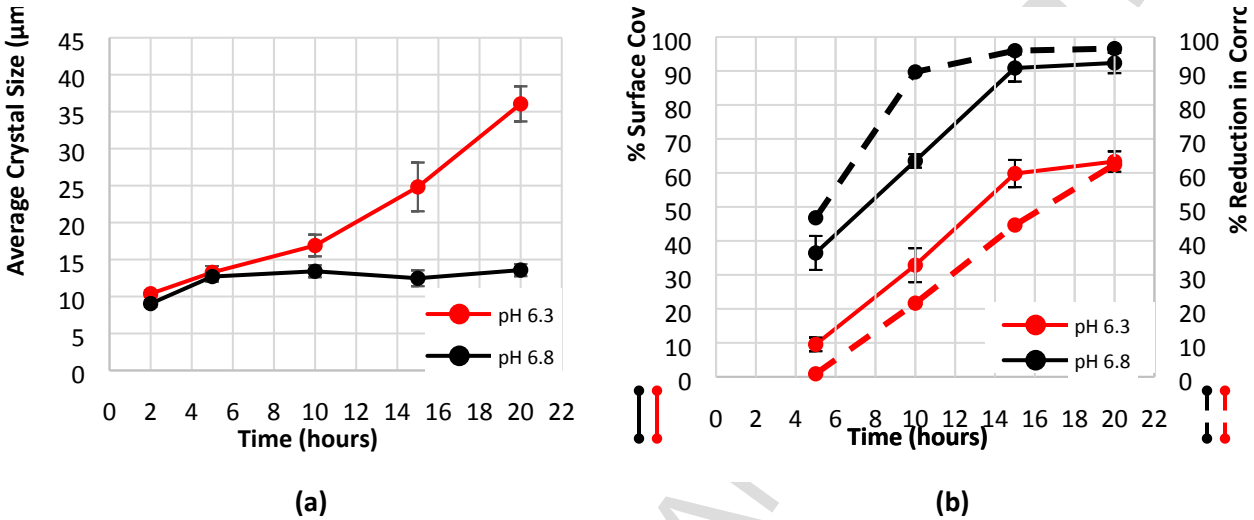

Figure 7. Analysis of SEM images from X65 carbon steel surfaces over time to determine (a) average crystal size (b) % surface coverage and % reduction in corrosion rate for pH 6.3 and pH 6.8.

The surface coverage shown in Figure 7(b) provides an estimate as to the percentage of the carbon steel surface covered with $FeCO_3$ crystals. This data was obtained through processing multiple SEM images from across the sample into a MATLAB program that utilizes the differences in contrast of the crystals formed against the bare steel surface to produce a binary output image. The program then plots the percentage of black pixels (crystals) against the white pixels (no crystals). The images selected for this analysis were captured at a lower magnification of ×80 in order to encompass a larger area of the sample and provide a more accurate representation of the overall surface coverage. The error bars show the extent of the variation in surface coverage determined by the program for the different images analyzed across the surface. The trend in surface coverage is observed to be very similar for pH 6.3 and pH 6.8 with it steadily increasing over time over 15 hours and then considerably slowing down thereafter. The surface coverage at pH 6.8 is found to be much higher at the end of each time period in comparison to pH 6.3, as expected given the lower final corrosion rate. After 20 hours, the surface coverage was determined to be approximately 92% at pH 6.8 and approximately 63% at pH 6.3. Observing the percentage reduction in the corrosion rate, determined from the mass loss measurements, Figure 7 (b) shows a reasonable agreement between the values obtained and the surface coverage. This indicates a direct relationship between the quantity of the mild steel surface covered by $FeCO_3$ crystals and the resulting decrease in the surface corrosion rate. The slight differences observed (~10% on average) may be attributed to limitations in the SEM images representing the overall sample surface. A top view coverage from SEM may not always correlate directly with the number of active sites physically blocked on the steel surface and may present limitations in capturing certain porosities between crystals.

The precipitation rate of $FeCO_3$ over time can be analytically calculated from the mass gain measurements over each time period. However, the equation, Equation (18), provides the integrated precipitation rate over a single time period, which inherently creates a limitation when attempting to accurately identify the change in precipitation kinetics with time. With this in mind, Equation (19) is a modified version of Equation (18) which considers the mass gain over time from one time period to the next (i.e. over discrete, shorter time intervals). This equation was used as opposed to Equation (18) in an attempt to provide a more accurate representation of the precipitation rate as a function of time.

$$PR = \frac{MG_{t2} - MG_{t1}}{MW_{FeCO3} \times t \times A \times 3600} \quad (19)$$

where PR is the precipitation rate (mol/m^2·s), MG_{t2}-MG_{t1} is the change in mass gain from one time interval to the next (g), MW_{FeCO3} is the molecular weight of $FeCO_3$ (in g/mol), t is the time interval in between measurements (h) and A is the exposed sample area (m^2).

Figure 8 shows the calculated precipitation rates for pH 6.3 and pH 6.8 and is plotted at the mid-point of each time interval. Results show that at pH 6.8, the precipitation rate increases to its highest value after 3.5 hours and then gradually decreases. In comparison, a similar trend is observed at pH 6.3. However, after a period of 5 hours, the precipitation rate at pH 6.3 overlaps with the precipitation rate at pH 6.8 and then steadily decreases but remains higher than that at pH 6.8. This observation correlates with the higher change in mass over time observed at pH 6.3 in Figure 4(a). An important observation is that there is not a dramatic difference in the precipitation rates between the two experiments. However, there is a significant difference from Figures 5 to 7 in relation to the manner in which the crystals nucleate and grow on the steel surface, along with the protection they afford. These observations imply that the precipitation rates do not directly correlate to the protective nature of the developed films.

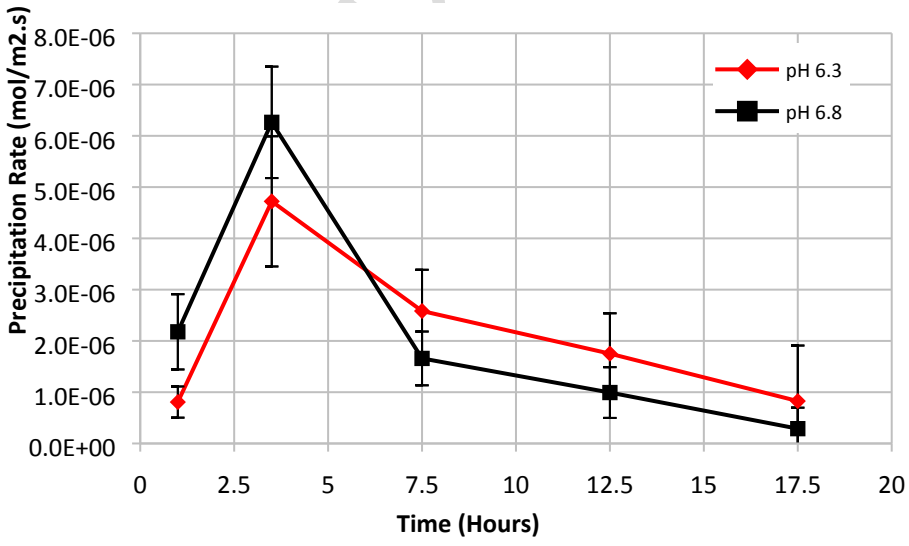

Figure 8. Precipitation rate (mol/m^2·s) of $FeCO_3$ onto X65 carbon steel calculated over time from mass gain measurements conducted at pH 6.3 and 6.8.

In literature [12-16], the precipitation rate of $FeCO_3$ has been frequently linked to the bulk solution chemistry/ saturation ratio. Figure 9 shows the measured Fe^{2+} ion concentration in the bulk solution over time and the resulting SR for both pH 6.3 and pH 6.8 determined according to Equation (15). The $FeCO_3$ solubility product, K_{sp}, for both pH 6.3 and pH 6.8 was calculated according to Equation (16) and determined to be 1.57×10^{-10} mol/L, independent of the solution pH.

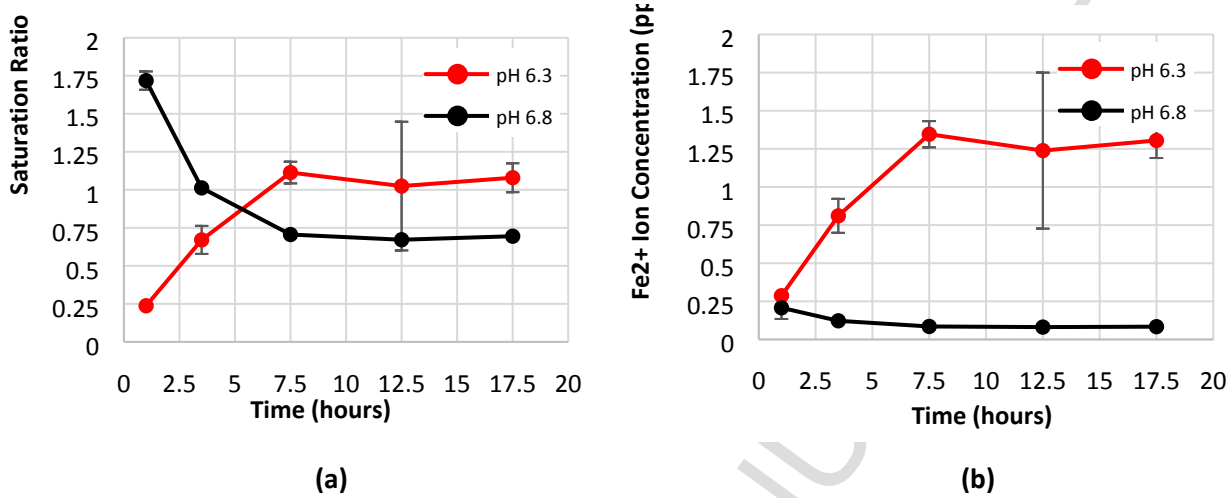

Figure 9. (a) Bulk SR over time determined from (b) bulk Fe^{2+} ion concentration through UV-spectroscopy for pH 6.3 and pH 6.8.

The figure shows that for pH 6.8, the initial bulk SR is observed to be approximately 1.7 and then decreases over the initial time periods settling at approximately 0.7 after 7.5 hours. At pH 6.3, the initial value of bulk SR is recorded at 0.2 and increases to approximately 1.1. After 7.5 hours, the bulk SR remains approximately constant with time at both conditions of pH. Reverting back to its calculation, Figure 9 (b) shows that at pH 6.8, the bulk Fe^{2+} ion concentration is approximately only 0.1 ppm at all time periods and a small decrease in the concentration results in a more significant corresponding change in the calculated SR as shown in Figure 9(a) from 1 to 3 hours. At pH 6.3, the Fe^{2+} ion concentration increases with time and then remains approximately the same after 7.5 hours. The results indicate that the bulk SR is observed to be very low in both experiments, remaining below 1.2 for the majority of both tests. Analysis of Figure 9 in comparison to Figure 8 reveals that precipitation is able to occur when the bulk solution is under-saturated with respect to $FeCO_3$. These observations suggest that the surface concentration of species (or surface SR) is particularly influential under these conditions as precipitation is thermodynamically not favorable in the bulk solution. Furthermore, the lack of any visible direct correlation between bulk SR and precipitation rate across both pH values in these experiments indicates that other factors are clearly influencing the precipitation rate for the low bulk SR systems, and that the bulk saturation ratio is not a main driving force for precipitation.

4. Discussion

4.1. Precipitation characteristics (rate and morphology)

Based on the experimental results, $FeCO_3$ crystals are observed to nucleate and grow simultaneously across the surface of the sample under both conditions of pH, yet the protectiveness of the developed film varies significantly. At pH 6.3, fewer crystals were observed on the surface but they were relatively larger

in size at each instance in time. At pH 6.8, the crystals were smaller in size but a larger quantity of crystals were observed on the surface. The reason behind the observed differences in the morphology of the scale can be related to the competition between the nucleation and growth processes.

According to crystallization theory [22,23], crystal nucleation poses a large energy barrier which is overcome at high levels of super-saturation, whereas crystal growth is limited by diffusion and existing stable nuclei. In a study by Arumugam et al. [24], the crystal nucleation rate, R_{Nuc} was defined as a function of saturation ratio, SR and is expressed in the form of Equation (20).

$$R_{Nuc} = P[A]exp\left[-\frac{16\pi\gamma^3 v^2}{3\left(kT_K\right)^3 \ln\left(SR\right)^2}\right] \quad (20)$$

Where P is the probability that [A] number of crystalizing solute nuclei will grow into crystals, γ is the the interfacial tension of the nucleated phase-solution boundary and T_K is the solution temperature. The study showed that a higher SR results in a higher nucleation rate and that corrosion product films are less porous and compact if the nucleation rate is higher than the growth rate. This suggests that the SR of the solution at pH 6.8 should be higher than that of pH 6.3 as significantly more crystal nucleation was observed.

As discussed previously, the SR for $FeCO_3$ is typically quantified based on the concentration of Fe^{2+} and CO_3^{2-} in the bulk. Considering the bulk solution chemistry, the equilibrium equations provided in Table 1 can be solved to determine bulk CO_3^{2-} ion concentrations of 7.70×10^{-5} mol/L for pH 6.8 and 7.70×10^{-6} mol/L for pH 6.3. Consequently, for the same concentration of Fe^{2+} ions in the bulk solution, the bulk SR is 10 times greater for a pH of 6.8 compared to 6.3. It is possible to loosely translate this to the conditions at the steel surface prior to precipitation. Referring back to Figures 2 and 4(b), the corrosion rate of X65 over the first 2 hours are very similar, indicating a similar surface flux/concentration of Fe^{2+} ions from/at the steel surface (at the very least of the same order of magnitude). Although the surface pH will be higher at the steel surface than the bulk solution due the corrosion process, the dramatic difference in CO_3^{2-} in the bulk solution is likely to be translated to the steel surface. Both these factors mean that a significantly higher surface SR will be generated at pH 6.8 compared to pH 6.3. This analogy can be used to explain the difference in characteristics of the film growth and morphology. Considering that nucleation varies exponentially with SR, while growth varies linearly with SR [25], less nucleation of crystals is expected at pH 6.3 and the existing Fe^{2+} ions contribute more to the growth of $FeCO_3$ crystals than at pH 6.8, which is only limited by diffusion and the number of existing stable nuclei. The higher surface SR at pH 6.8 results in the ionic species contributing more strongly to nucleation than at pH 6.3, leaving less Fe^{2+} ions available for crystal growth, resulting in a more extensive layer of crystals with a smaller average diameter. Consequently, the SEM observations of crystal growth agree well with the anticipated differences in surface SR at each pH.

4.2. Role of surface coverage on precipitation rate

In Figure 8, after a period of 3 hours, the precipitation behavior of $FeCO_3$ was observed to decrease over time at both conditions of pH studied with the further development of the $FeCO_3$ film and increasing surface coverage. Furthermore, comparing Figures 2 and 8, the results show that the protectivity of the developed film is irrespective of the quantity of $FeCO_3$ present on the mild steel surface. To further

understand the $FeCO_3$ precipitation behavior at the steel-electrolyte interface, it is important to revert back to its calculation which is essentially, the change in mass gain observed in Figure 4(a) and the results from the surface analysis shown in Figures 5 and 6.

At the early time stages, Figures 6 (a) and (b) show that a larger quantity of $FeCO_3$ crystals were observed to be present at pH 6.8 in comparison to pH 6.3 (Figures 5 (a) and (b)) with relatively the same average crystal size. However, over time, despite the surface analysis showing a higher quantity of $FeCO_3$ crystals on the surface at pH 6.8, the more predominant growth process at pH 6.3 resulted in significantly larger crystals on the surface as indicated in Figure 7 (a). The complex morphology of the $FeCO_3$ film formation limits mass gain measurements to a simple analysis of the total $FeCO_3$ that forms on the surface. At the end of 20 hours, as shown in Figure 4 (a), the mass gain at pH 6.3 was observed to be higher than pH 6.8 even though a significantly larger percentage surface coverage was observed at pH 6.8. This implies that the total mass of the larger, fewer crystals formed at pH 6.3 was more significant than the total mass of the many, larger crystals formed at pH 6.8. Consequently, this higher change in mass observed from one time period to the next at pH 6.3 translates to the higher precipitation rate recorded at pH 6.3 after 7.5 hours limiting the significance of the calculated precipitation rate and its link to the protectiveness of the developed film.

In Figure 10, the experimental precipitation rate results beyond 7.5 hours is plotted against the surface coverage and the percentage reduction in corrosion rate. The figure shows that the precipitation rate reduces in conjunction with increased surface coverage and the percentage reduction in the corrosion rate at both pH 6.3 and pH 6.8. This is attributed to the fact that active sites on the steel surface become blocked by the crystals, suppressing SR locally and reducing precipitation rate at discrete locations. As the surface coverage increases, the consequent reduction in the corrosion rate is expected to reduce the availability of Fe^{2+} ions and the SR required to meet the energy barrier required for the nucleation and further growth of $FeCO_3$ crystals.

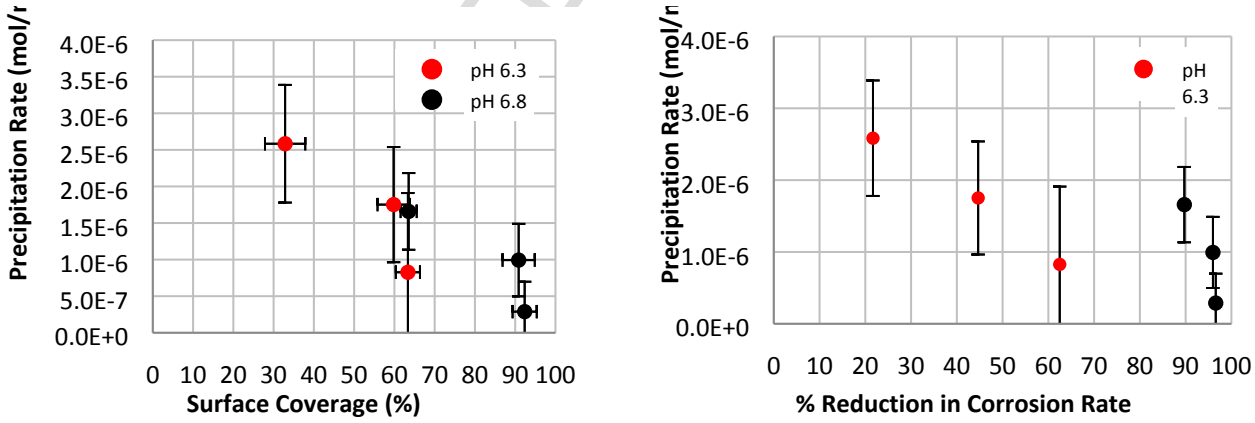

Figure 10. Precipitation rate (mol/m²·s) as a function of (a) surface coverage and (b) percentage reduction in corrosion rate for pH 6.3 and 6.8.

4.3. Retention of Fe^{2+} at the steel surface and scaling tendency

Comparing Figures 2 and 9(b), the analytically calculated Fe^{2+} ion concentration in the bulk solution is significantly higher than that which was measured using spectrophotometry. This is to be expected as the values in Figure 2 do not account for precipitation within the system. Figure 11 shows the percentage of Fe^{2+} ions emitted into the solution which are precipitated back onto the steel surface at each pH and different time periods. This information is essentially the ratio of the precipitation rate to the corrosion rate expressed as a percentage and is referred to by Nesic et al. [13] as the scaling tendency.

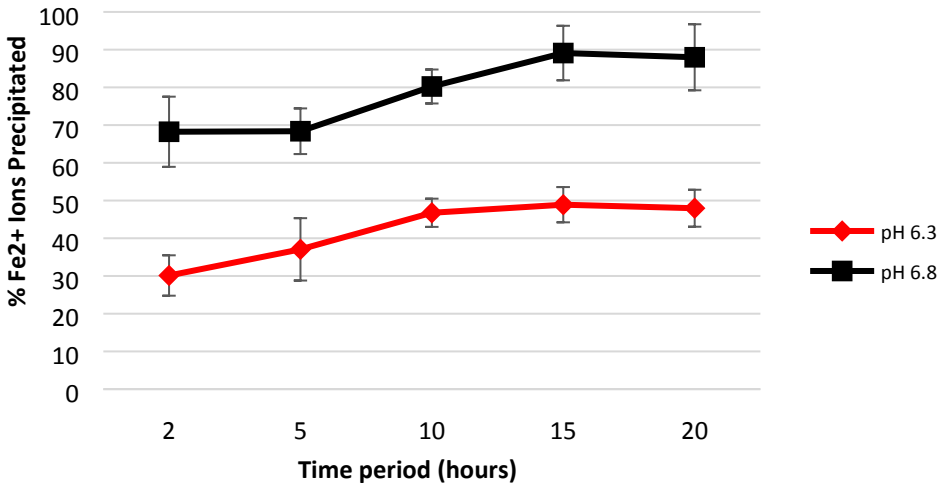

Figure 11. % Fe^{2+} ions lost from surface that precipitate as $FeCO_3$ back onto the steel surface, determined from mass change results and bulk solution Fe^{2+} measurements.

Figure 11 shows that over a time period of 2, 5, 10, 15 and 20 h from the beginning of the experiment, a significantly higher percentage of Fe^{2+} ions produced due to corrosion is precipitated as $FeCO_3$ at a pH 6.8 than at pH 6.3. On average, the percentage of Fe^{2+} ions 'retained' at the surface is approximately 77.4% at pH 6.8 and 43% at pH 6.3 (i.e. scaling tendencies of 0.77 and 0.43). Under the following conditions of the CO_2 corrosion process, there is competition between the diffusion of Fe^{2+} ions away from the surface and precipitation back onto the surface. It may be inferred that a higher pH results in a higher surface SR, faster precipitation and hence, greater retention of Fe^{2+} at the surface in the form of $FeCO_3$. The remaining percentage of Fe^{2+} ions lost from the surface, unaccounted for in Figure 11, may be the results of bulk precipitation elsewhere in the cell and Fe^{2+} ions in the bulk solution. The lower percentage of Fe^{2+} ions precipitated at pH 6.3 provides an explanation for the higher bulk Fe^{2+} ion concentrations observed in Figure 9 (b) in comparison to pH 6.8.

In the work by Nesic et al.[12,13], much of the research was carried out with the addition of $FeCl_2.4H_2O$ to accelerate the kinetics of $FeCO_3$ film formation. This is more representative of downstream in a pipeline where bulk Fe^{2+} ions may influence the surface formation of $FeCO_3$. It is noted subsequently that a scaling tendency of greater than one is believed to be indicative of protective film formation. However, in the following work, for a freely corroding system representing the early stages of film growth, a relatively protective film is obtained at a pH 6.8 after 20 hours and in these conditions, a scaling tendency of greater than one is never reached.

5. Conclusions

In the following research, the complex nucleation and growth process of iron carbonate was studied to understand the factors conducive to protective film formation. The following conclusions can be drawn from the results and discussion of this work:

- For a freely corroding steel surface, in CO_2 saturated static conditions, $FeCO_3$ precipitation was observed when the bulk solution SR < 1. This indicates that local surface conditions are very different than those in the bulk solution and the precipitation rate of $FeCO_3$ cannot be directly correlated with bulk solution properties.
- A significantly more protective corrosion film is observed to have developed at pH 6.8 in comparison with pH 6.3 at the end of 20 hours. The root cause of this difference in the characteristics of the developed film is proposed to be largely associated with the dramatic difference in the CO_3^{2-} ion concentration at varying pH.
- Surface analysis (SEM) shows that $FeCO_3$ nucleation and growth is a simultaneous process. The competition between the nucleation and growth of $FeCO_3$ crystals as a result of surface conditions results in differences in the precipitated film. At a higher pH, the more protective film formed is associated with a more compact and dense crystal formation. Under lower pH conditions, a more dominant growth process results in fewer nucleation of crystals and more surface regions uncovered by a protective film.
- Surface coverage of crystals, total Fe^{2+} flux from the steel surface and local SR play an important role in the initial precipitation kinetics of $FeCO_3$.
- Mass gain (quantitative analysis) does not directly relate to the protectiveness of the $FeCO_3$ films.
- Scaling tendency is a valid indicator of protective film formation. A high scaling tendency appears to favor the formation of dense, protective iron carbonate films.

Acknowledgments

The authors wish to acknowledge the financial support from sponsors, BP.

References

1. Papavinasam, S., *Corrosion control in the Oil and Gas Industry*. Gulf Professional Publishing, Amsterdam, 2013.
2. Nordsveen, M., S. Nesic, R. Nyborg, and A. Stangeland, *A mechanistic model for carbon dioxide corrosion of mild steel in the presence of protective iron carbonate films-Part 1: Theory and verification*. Corrosion, 2003. **59**(5): p. 443-456.
3. Oddo, J.E. and M.B. Tomson, *Simplified Calculation of $CaCO_3$ Saturation at High Temperatures and Pressures in Brine Solutions*. Journal of Petroleum Technology, 1982. **34**(07): p. 1,583-1,590.
4. Palmer, D.A. and R. Van Eldik, *The chemistry of metal carbonate and carbon dioxide complexes*. Chemical Reviews, 1983. **83**(6): p. 651-731.
5. De Waard, C. and D. Milliams, *Carbonic acid corrosion of steel*. Corrosion, 1975. **31**(5): p. 177-181.
6. Kermani, M. and A. Morshed, *Carbon dioxide corrosion in oil and gas production - A compendium.* Corrosion, 2003. **59**(8): p. 659-683.

7. Nesic, S., M. Nordsveen, and A. Stangeland, *A Mechanistic Model for CO_2 Corrosion with Protective Iron Carbonate Films.* in: NACE Corrosion 2001: Paper no. 01040.
8. Nesic, S., J. Postlethwaite, and S. Olsen, *An electrochemical model for prediction of corrosion of mild steel in aqueous carbon dioxide solutions*. Corrosion, 1996. **52**(4): p. 280-294.
9. Remita, E., B. Tribollet, E. Sutter, V. Vivier, F. Ropital and J. Kittel, *Hydrogen evolution in aqueous solutions containing dissolved CO_2: Quantitative contribution of the buffering effect*. Corrosion Science, 2008. **50**(5): p. 1433-1440.
10. Bockris, J., D. Drazic, and A. Despic, *The Electrode Kinetics of the Deposition and Dissolution of Iron.* Electrochimica Acta, 1961. **4**(2-4): p. 325-361.
11. Zheng, Y., J. Ning, B. Brown, and S. Nesic, *Advancement in predictive modeling of mild steel corrosion in CO_2 and H_2S containing environments*. Corrosion, 2016. **72**(5): p. 679-691.
12. Sun, W., *Kinetics of iron carbonate and iron sulfide scale formation in CO_2/H_2S corrosion*. PhD Thesis, Ohio University, 2006.
13. Sun, W. and S. Nesic, *Basics revisited: kinetics of iron carbonate scale precipitation in CO_2 corrosion*. in: NACE Corrosion 2006: Paper no. 06365.
14. Greenberg, J. and M. Tomson, *Precipitation and dissolution kinetics and equilibria of aqueous ferrous carbonate vs temperature*. Applied Geochemistry, 1992. **7**(2): p. 185-190.
15. Johnson, M. and M. Tomson, *Ferrous Carbonate Precipitation Kinetics and its Impact on CO_2 Corrosion*. in: NACE Corrosion 1991: Paper no. 268.
16. Van Hunnik, E., B. Pots, and E. Hendriksen, *The Formation of Protective Corrosion Product Layers in CO_2 Corrosion*. in: NACE Corrosion 1996: Paper no. 96006.
17. Wei, L., B. Brown, D. Young and S. Nesic, *Investigation of Pseudo-Passivation of Mild Steel in CO_2 Corrosion*. Corrosion, 2014. **70**(3): p. 294-302.
18. Tanupabrungsun, T., B. Brown, and S. Nesic, *Effect of pH on CO_2 corrosion of mild steel at elevated temperatures*. in: NACE Corrosion 2013: Paper no. 2348.
19. Schmitt, G. and M. Horstemeier, *Fundamental aspects of CO_2 metal loss corrosion-Part II: Influence of different parameters on CO_2 corrosion mechanisms*. in: NACE Corrosion 2006: Paper no. 06112.
20. Stern, M. and A. Geary, *Electrochemical polarization I. A theoretical analysis of the shape of polarization curves*. Journal of the Electrochemical Society, 1957. **104**(1): p. 56-63.
21. Bockris, J., D. Drazic, and A.R. Despic, *The Electrode Kinetics of the Deposition and Dissolution of Iron*. Electrochimica Acta, 1961. **4**(2-4): p. 325-361.
22. Markov, I.V. *Crystal growth for beginners: fundamentals of nucleation, crystal growth and epitaxy*. World Scientific, Singapore, 2003.
23. Meenan, P., *From Molecules to Crystallizers An Introduction to Crystallization*. Crystal Growth & Design, 2001. **1**(1): p. 101-101.
24. Arumugam, S., N. Tajallipour, and P. Teevens. *Modeling the Nucleation and Growth of Corrosion Scales in Sour Petroleum Pipelines*. in: NACE Corrosion 2014: Paper no. 4326.
25. Nešić, S., *Key issues related to modelling of internal corrosion of oil and gas pipelines–A review.* Corrosion Science, 2007. **49**(12): p. 4308-4338.

Highlights

- Investigation of the nucleation and growth process of $FeCO_3$ crystals.
- Experiments conducted in static conditions conducive to protective film formation.
- Influence of pH on $FeCO_3$ precipitation kinetics is identified.
- Significance of surface properties in relation to bulk solution properties was investigated.
- Film development over time is observed to identify characteristics of crystal growth.